Orientational Ordering, Buckling, and Dynamic Transitions for Vortices Interacting with a Periodic Quasi-One Dimensional Substrate

Q. Le Thien[1,2], D. McDermott[1,2], C. J. Olson Reichhardt[1], and C. Reichhardt[1]

[1]*Theoretical Division, Los Alamos National Laboratory, Los Alamos, New Mexico 87545 USA*
[2]*Department of Physics, Wabash College, Crawfordsville, Indiana 47933 USA*

(Dated: August 25, 2015)

We examine the statics and dynamics of vortices in the presence of a periodic quasi-one dimensional substrate, focusing on the limit where the vortex lattice constant is smaller than the substrate lattice period. As a function of the substrate strength and filling factor, within the pinned state we observe a series of order-disorder transitions associated with buckling phenomena in which the number of vortex rows that fit between neighboring substrate maxima increases. These transitions coincide with steps in the depinning threshold, jumps in the density of topological defects, and changes in the structure factor. At the buckling transition the vortices are disordered, while between the buckling transitions the vortices form a variety of crystalline and partially ordered states. In the weak substrate limit, the buckling transitions are absent and the vortices form an ordered hexagonal lattice that undergoes changes in its orientation with respect to the substrate as a function of vortex density. At intermediate substrate strengths, certain ordered states appear that are correlated with peaks in the depinning force. Under an applied drive the system exhibits a rich variety of distinct dynamical phases, including plastic flow, a density-modulated moving crystal, and moving floating solid phases. We also find a dynamic smectic-to-smectic transition in which the smectic ordering changes from being aligned with the substrate to being aligned with the external drive. The different dynamical phases can be characterized using velocity histograms and the structure factor. We discuss how these results are related to recent experiments on vortex ordering on quasi-one-dimensional periodic modulated substrates. Our results should also be relevant for other types of systems such as ions, colloids, or Wigner crystals interacting with periodic quasi-one-dimensional substrates.

PACS numbers: 74.25.Wx,74.25.Uv,74.25.Ha

I. INTRODUCTION

Commensurate-incommensurate transitions are relevant to a number of condensed matter systems that can be effectively described as a lattice of particles interacting with an underlying periodic substrate. A commensurate state occurs when certain length scales of the particle lattice match the periodicity of the underlying substrate, such as when the number of particles is equal to the number of substrate minima[1,2]. Typically when commensurate conditions are met, the system forms an ordered state free of topological defects, while at incommensurate fillings there are several possibilities depending on the strength of the substrate. If the substrate potential is weak, the particles maintain their intrinsic lattice structure which floats on top of the substrate, while for strong substrates a portion of the particles lock into a configuration that is commensurate with the substrate while the remaining particles form excitations such as kinks, vacancies, or domain walls. At intermediate substrate strengths, the lattice ordering can be preserved but there can be periodic distortions or rotations of the particle lattice with respect to the substrate lattice[3–8]. These different cases are associated with differing dynamical responses of the particles under the application of an external drive[2,7–11]. When kinks or domain walls are present, multi-step depinning process can occur when the kinks become mobile at a lower drive than the commensurate portions of the sample[7,8]. Examples of systems that exhibit commensurate-incommensurate phases include atoms adsorbed on atomic surfaces[1,3,4], vortices in type-II superconductors interacting with artificial pinning arrays[12–21], vortex states in Josephson-junction arrays[22,23], superfluid vortices in Bose-Einstein condensates in the presence of co-rotating optical trap arrays[24–26], cold atoms and ions on ordered substrates[27–30], and colloidal particles on periodic[6–8,31–34] and quasi-periodic optical substrates[35,36].

In the superconducting vortex system, commensurability occurs when the number of vortices is an integer multiple of the number of pinning sites, and various types of commensurate vortex crystalline states can occur with different symmetries[12,13,16,19]. At fillings where there are more vortices than pinning sites, it is possible to have multi-quantized vortices occupy the pinning sites, and a composite vortex lattice can form that is comprised of individual or multiple flux-quanta vortices localized on pinning sites coexisting with vortices located in the interstitial regions between the pinning sites[12,19,20]. Ordered commensurate vortex states have been directly imaged with Lorentz microscopy[13] and other imaging techniques[37,38], and the existence of commensuration can also be deduced from changes in the depinning force needed to move the vortices when peaks or steps appear in the critical current as a function of vortex density[12,14–16,18,19]. It is also possible for ordered vortex structures such as checkerboard states to form at rational fractional commensuration ratios of n/m with integer m and n, where n is the number of vortices and

m is the number of pinning sites[37–40]. Experiments[7] and simulations[8,41] of colloidal assemblies on optical trap arrays examined the depinning transitions and subsequent sliding of the colloids and show that the depinning threshold is maximum for one-to-one matching of colloids and traps, while it drops at incommensurate fillings due to the presence of highly mobile kinks, anti-kinks, and domain walls.

Commensurate-incommensurate transitions can also occur for particles interacting with a periodic quasi-one-dimensional (q1D) or washboard potential, where the particles can slide freely along one direction of the substrate but not the other. An example of this type of system is shown in Fig. 1 for a two-dimensional system of vortices interacting with a quasi-one dimensional sinusoidal substrate. The potential maxima are indicated by the darker shadings, and the vortices are attracted to the light colored regions. This type of system has been studied previously for colloids interacting with q1D periodic substrate arrays, where it was shown that various melting and structural transitions between hexagonal, smectic, and disordered colloidal arrangements can occur[42–48]. In general, the colloidal studies focused on the case where the particle lattice constant a is larger than the substrate lattice constant w. Martinoli *et al.* investigated vortex pinning in samples with a 1D periodic thickness modulation[49–51] and observed broad commensuration peaks in the depinning threshold that were argued to be correlated with the formation of ordered vortex arrangements that could align with the substrate periodicity. Other vortex studies in similar samples also revealed peaks in the critical depinning force associated with commensuration effects[52,53], while studies of vortices interacting with 1D magnetic strips showed that commensurate conditions were marked by depinning steps rather than peaks[54]. Under an applied dc drive, depinning transitions occur into a sliding state, and when an additional ac drive is added to the dc drive, a series of Shapiro steps in the voltage-current curves appears when the frequency of the oscillatory motion of the vortex lattice over the periodic substrate locks with the ac driving frequency[50]. Similar commensuration effects and Shapiro step phenomena were also studied for vortices interacting with periodic washboard potentials or q1D periodic sawtooth substrates[55]. Vortices interacting with periodic q1D planar defects have also been studied in layered superconductors when the field is aligned parallel to the layer directions. Here, different vortex lattice structures, smectic states, and oscillations in the critical current occur as a function of applied magnetic field[56–62].

For higher vortex densities in the presence of a q1D substrate where the vortex lattice constant a is *smaller* than the substrate lattice constant, $a < w$, there are several possibilities for how the vortices can order. In the weak substrate limit, they can form a hexagonal lattice containing only small distortions, while in the strong substrate limit the vortices can be strongly confined in each potential minimum to form 1D rows, so that the over-
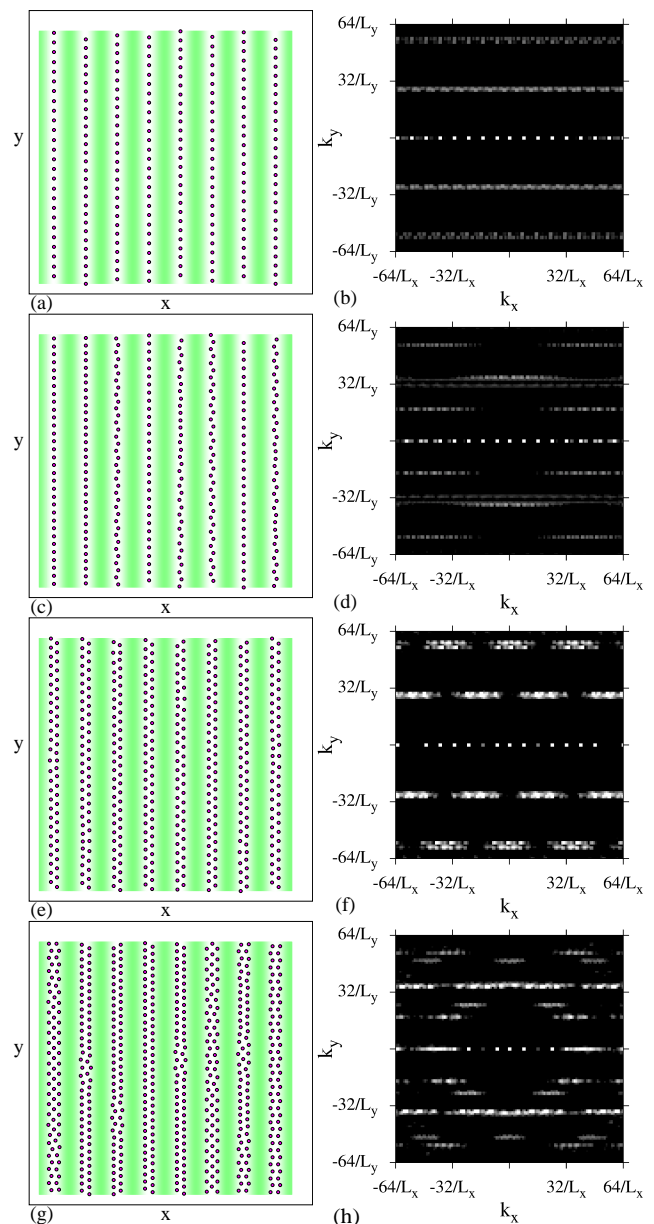

FIG. 1: The real space images (left column), with the substrate minima indicated by lighter regions and the vortex positions marked with circles, and the structure factor $S(k)$ (right column), for a system with a periodic quasi-one-dimensional substrate with $F_p = 1.5$. (a,b) At $w/a = 1.85$, each substrate minimum contains a single row of vortices (r_1) and the structure factor shows smectic order. (c,d) $w/a = 2.054$, at the onset of a buckling transition. (e,f) At $w/a = 2.651$ there is an ordered zig-zag r_2 vortex lattice. (g,h) At $w/a = 3.0$ there is a mixture of r_2 and r_3 lattices.

all two-dimensional (2D) vortex structure is anisotropic. Between these limits, the vortices can exhibit buckling transitions by forming zig-zag patterns within individual potential troughs, so that for increasing vortex density there could be a series of transitions at which increasing numbers of rows of vortices appear in the potential

troughs. Transitions from 1D rows of particles to zig-zag states or multiple rows have been studied for particles in single q1D trough potentials in the context of vortices[63–65], Wigner crystals[66–68], colloids[70,70–72], q1D dusty plasmas[73,74], ions in q1D traps[75–77], and other systems[78,79] where numerous structural transitions, diffusion behavior and dynamics can occur. In the case of a periodic array of channels such as shown in Fig. 1, much less is known about what buckling transitions would occur and what the dynamics would be under an applied driving force. Recently Guillamón *et al.* studied vortex lattices in samples with a periodic q1D array of grooves. As a function of the commensuration ratio $p = w/a$, they found that for $p < 6$, the vortex lattice remains triangular but undergoes a series of transitions that are marked by rotations of the angle θ made by the vortex lattice with respect to the substrate symmetry direction[80]. They also observed that at much higher fields, the system transitions into a disordered state with large vortex density fluctuations. Open questions include what happens to these reorientation transitions as the substrate strength is increased, and what the vortex dynamics are when a driving force is applied. Dynamical phases and structural transitions between different kinds of nonequilibrium vortex flow states have been extensively studied for driven vortex systems interacting with random[81–86] and 2D periodic pinning arrays[87–89]; however, there is very little work examining the dynamic vortex phases for vortices moving over q1D periodic substrates. It is not known whether the vortices would undergo dynamical structural transitions or exhibit the same types of dynamic phases found for vortices driven over random disorder, such as a disordered plastic flow state that transitions to a moving smectic or anisotropic crystal as a function of increasing drive.

In this work we consider ordering and dynamics of vortices interacting with a periodic q1D sinusoidal potential for fillings $0 < w/a < 5.5$. In the strong substrate regime, the system undergoes a series of structural transitions that are related to the number of rows r_n of vortices that fit within each substrate trough. These transitions include transformations from 1D vortex rows to zig-zag patterns that gradually increase r_n. The vortex structure contains numerous dislocations at the buckling transitions and is ordered between the buckling transitions. For strong substrates, the onset of the buckling and ordered phases produces a series of steps in the critical depinning threshold as a function of vortex density, while for weaker substrate strengths, some of the states in which the vortices order produce peaks in the critical depinning force. For the weakest substrates, the vortices form a triangular lattice that undergoes rotations with respect to the underlying substrate symmetry direction as a function of applied magnetic field, similar to the behavior observed by Guillamon *et al.*[80]. Under an applied drive we observe plastic flow states, moving density-modulated crystals, and dynamic floating solids. For certain fillings we also find smectic-to-smectic transitions where the two

smectic states have different orientations. These different flowing phases produce distinct features in the velocity histograms and the structure factor. The commensurability ratio w/a also strongly affects the driving force at which the transition to a moving floating solid occurs. Our results should be general to other types of systems that can be represented as a collection of repulsive particles interacting with a periodic q1D substrate, such as colloids on optical line traps, ions in coupled traps, and Wigner crystals on corrugated substrates.

II. SIMULATION

We model a two-dimensional system of vortices interacting with a periodic q1D potential with period w, where there are periodic boundary conditions in the x and y-directions. The vortices are modeled as point particles and the dynamics of an individual vortex i obeys the following equation of motion:

$$\eta \frac{d\mathbf{R}_i}{dt} = \mathbf{F}_{vv}^i + \mathbf{F}_i^s + \mathbf{F}_d^i + \mathbf{F}_T^i. \tag{1}$$

Here η is the damping constant which we set equal to unity. The vortex-vortex forces $\mathbf{F}_{vv}^i = \sum_{j=1}^{N_v} F_0 K_1(R_{ij}/\lambda)\hat{\mathbf{R}}_{ij}$, where $F_0 = \phi_0^2/2\pi\mu_0\lambda^3$, ϕ_0 is the elementary flux quantum, μ is the permittivity, K_1 is the modified Bessel function, $\mathbf{R}_i$ is the location of vortex i, $R_{ij} = |\mathbf{R}_i - \mathbf{R}_j|$, $\hat{\mathbf{R}}_{ij} = (\mathbf{R}_i - \mathbf{R}_j)/R_{ij}$, and λ is the penetration depth. The vortices have repulsive interactions and form a triangular lattice in the absence of a substrate. The vortex interaction with the substrate is given by $\mathbf{F}_i^s = -\nabla V(x_i)\hat{\mathbf{x}}$ where the substrate has the sinusoidal form

$$V(x) = V_0 \sin(2\pi x/w). \tag{2}$$

We define the pinning strength of the substrate to be $F_p = 2\pi V_0/w$. The dc driving force $\mathbf{F}_d^i$ arises from the Lorentz force induced by a current applied along the easy direction (y-axis) of the substrate which produces a perpendicular force on the vortices and causes them to move in the x-direction in our system. We measure the vortex velocity $\langle V_x \rangle$ along the driving direction as we increase the external drive in increments of δF_d, and average the vortex velocities over a fixed time in order to avoid any transient effects. The thermal forces $\mathbf{F}_T$ are modeled as random Langevin kicks with the properties $\langle \mathbf{F}_T \rangle = 0$ and $\langle \mathbf{F}_T^i(t)\mathbf{F}_T^j(t') \rangle = 2\eta k_B T \delta_{ij}\delta(t - t')$, where k_B is the Boltzmann constant. The initial vortex positions are obtained by annealing from a high temperature state and cooling down to $T = 0$. The dc drive is applied only after the annealing procedure is completed. We consider a range of vortex densities, which we report in terms of the ratio w/a of the periodicity of the substrate to the vortex lattice constant that would appear in the absence of a substrate. We denote a state containing n rows of vortices in each potential minimum as r_n.

FIG. 3: The fraction of six-fold coordinated vortices P_6 vs w/a for (a) $F_p = 0.5$, (b) $F_p = 1.0$, (c) $F_p = 1.5$ and (d) $F_p = 2.0$. In panel (c), the labels a, c, e, g indicate the values of w/a at which the images in Fig. 1 were obtained, while the labels A, C, E, and G indicate the values of w/a at which the images in Fig. 2 were obtained. The dips in P_6 coincide with transitions in the number of vortex rows contained within each potential minimum.

the corresponding structure factor shown in Fig. 2(f). At higher fields, the vortex structures become disordered as shown in Fig. 2(g) at $w/a = 5.15$, where $S(k)$ in Fig. 2(h) has pronounced ring structures. There are still two peaks at $k_y = 0$ and finite k_x due to the smectic ordering imposed by the q1D substrate.

We can also characterize the system using the fraction of six-fold coordinated vortices $P_6 = N^{-1} \sum_{i=1}^{N} \delta(6 - z_i)$, where z_i is the coordination number of vortex i obtained from a Voronoi construction. In general, we find that P_6 drops at the buckling transitions due to the formation of dislocations that are associated with the splitting of a single row of vortices into two rows, creating a kink at the intersection of the two rows. In Fig. 3(a) we plot P_6 versus w/a for a system with $F_p = 0.5$. Over the range $1.0 < w/a < 1.7$, each pinning trough contains an r_1 state, while the dip in P_6 at $w/a = 1.77$ corresponds to the middle of the buckling transition when there is roughly a 50:50 mixture of r_1 and r_2. For $1.85 < w/a < 2.35$, the system forms an ordered r_2 state sim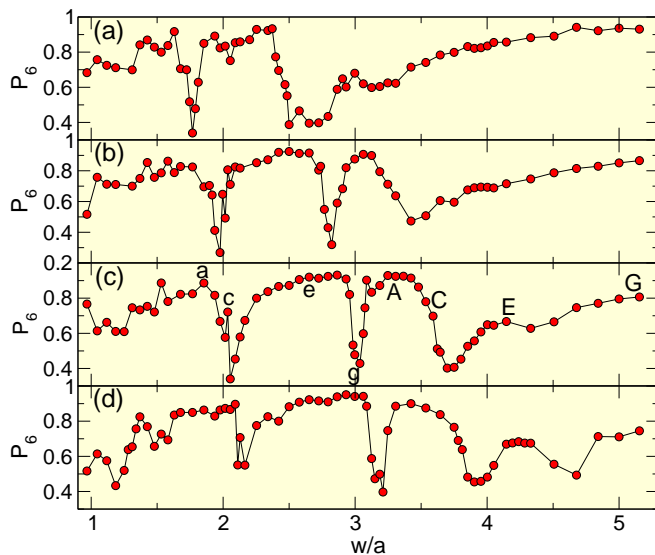ilar to that shown in Fig. 1(e), but less anisotropic since the weaker substrate compresses the zig-zag structure less and permits it to be wider. Near $w/a = 2.4$, there is another buckling transition from r_2 to r_3 and the system forms a disordered state similar to that shown in Fig. 1(g). As w/a is further increased, there is a partially ordered state near $w/a = 3$ that is similar to the state in Fig. 2(a); however, due to the weaker substrate strength a fully ordered r_3 state does not form. For $w/a > 3.2$ the

system adopts a polycrystalline configuration that becomes more ordered at high vortex densities. In Fig. 3(b), we show that a similar set of features associated with buckling transitions occurs for a stronger substrate with $F_p = 1.0$; however, in this case the transition from r_2 to r_3 is sharper and a fully ordered three row state appears near $w/a = 3.0$.

In Fig. 3(c) we plot P_6 versus w/a for samples with $F_p = 1.5$, the same pinning strength at which the images in Figs. 1 and 2 were obtained. Here the dips in P_6 associated with the r_1 to r_2, r_2 to r_3, and r_3 to r_4 transitions are sharper. We also observe the development of a small dip near $w/a = 4.4$ corresponding to a partial transition from r_4 to r_5. The values of w/a at which row transitions occur shift upward with increasing F_p. For example, the r_1 to r_2 transition occurs at $w/a = 1.768$ for $F_p = 0.5$ but at $w/a = 2.05$ for $F_p = 1.5$, since the higher F_p stabilizes the r_1 state up to higher lattice constant anisotropies. Figure 3(d) shows P_6 versus w/a for samples with $F_p = 2.0$. Here the dip in P_6 at the r_1 to r_2 transition broadens, while a pronounced jump emerges at $w/a = 4.7$ corresponding to the r_4 to r_5 transition. We expect that for higher values of F_p, additional dips in P_6 for transitions from r_n to r_{n+1} states for $n \geq 5$ will appear at w/a values higher than those we consider here.

It is difficult to determine if the buckling transitions are first or second order in nature. For particles in an isolated trough, the transition from a single row to a zig-zag pattern is second order, and there have been several studies in cold ion systems of quenches through this transition in which the density of kinks was calculated for different quench rates and compared to predictions from nonequilibrium physics on quenches through continuous phase transitions[75–77]. We expect that the buckling transitions we observe are second order; however, it may be possible that the additional coupling to particles in neighboring potential minima could change the nature of the transition, and we have observed a coexistence of chain states which is suggestive of phase separation. For vortex systems it could be difficult to change the substrate strength as a function of time, but for colloidal systems it is possible to create q1D periodic optical substrates of adjustable depth and use them to study time dependent transitions by counting the number of kinks that form as a function of the rate at which the substrate strength is changed.

In Fig. 4 we plot the depinning force F_c versus w/a for $F_p = 0.1, 0.25, 0.5, 1.0, 1.5,$ and 2.0 to show that the buckling transitions are associated with changes in the slope of the depinning force, which decreases with increasing w/a in a series of steps. The first drop in F_c near $w/a = 2.0$ corresponds to the r_1 to r_2 transition. In the r_1 state, the particle-particle interactions roughly cancel in the x-direction, so the depinning force is approximately equal to F_p, while close to the buckling transition the vortices on the right side of a zig-zag experience an additional repulsive force in the driving direction from the vortices on the left side of the zig-zag, decreasing the
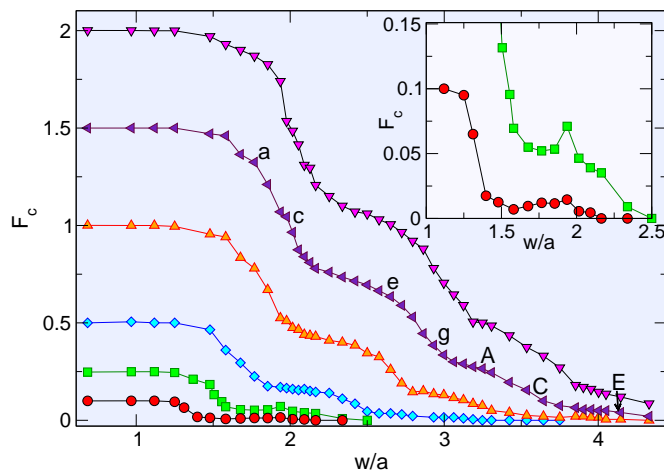
FIG. 4: The depinning force F_c vs w/a for $F_p = 0.1$ (red circles), 0.25 (green squares), 0.5 (blue diamonds), 1.0 (orange up triangles), 1.5 (purple left triangles), and 2.0 (pink down triangles) showing that for $F_p > 0.25$ the buckling transitions correspond to step features in F_c. The labels a, c, e, g indicate the values of w/a at which the images in Fig. 1 were obtained, while the labels A, C, and E indicate the values of w/a at which the images in Fig. 2 were obtained. Inset: a highlight of the main panel illustrates that for weaker pinning, peaks in F_c occur, as shown for $F_p = 0.1$ (red circles) and 0.25 (green squares). The peak is associated with the formation of an ordered zig-zag lattice similar to that shown in Fig. 1(e).
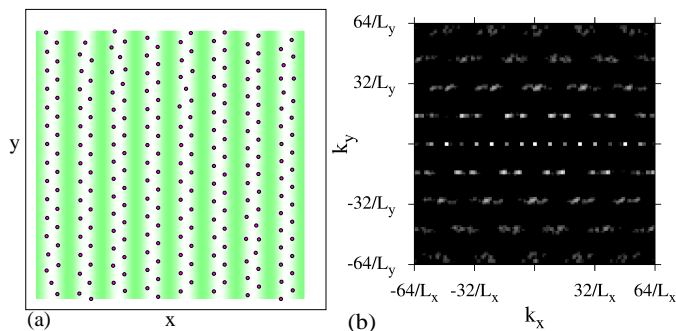

FIG. 5: (a) Real space image of the vortex configuration at the peak in F_c at $F_p = 0.25$ and $w/a = 1.94$ for the system shown in the inset of Fig. 4 where an ordered zig-zag structure occurs. (b) The corresponding $S(k)$ contains various peaks reflecting the ordered nature of the state.

driving force needed to depin the vortices. To estimate the magnitude of this reduction in F_c, we note that the average x-direction spacing between vortices in a given zig-zag is approximately $d_x = 2.0$. For a zig-zag with a $30°$ angle between the two closest neighbors on the other side of the chain from each vortex, the vortex-vortex interaction force of $K_1(2)$ produces an additional repulsive force of $f_r = 0.55$, giving a value of $F_c = F_p - f_r$ that is close to the value of $F_c = 0.78$ observed after the r_1 to r_2 step for the $F_p = 1.5$ system. Similar arguments can be made for the magnitudes of the drops in F_c at the higher

order transitions as well. At $w/a = 1.85$ in the $F_p = 1.5$ sample, F_c already begins to drop below F_p even though the pinned configuration shown in Fig. 1(a) is an r_1 state. This occurs because in this range of w/a, application of a finite $F_d < F_c$ induces a slight buckling of the vortices, while for $w/a < 1.5$ the r_1 rows remain in a 1D pinned state up to $F_d = F_c$. The inset of Fig. 4 shows a blowup of F_c versus w/a for the weaker pinning cases $F_p = 0.25$ and $F_p = 0.1$. At $w/a = 1.94$ there is a peak in F_c for the $F_p = 0.25$ sample coinciding with the formation of the long range ordered zig-zag state shown in Fig. 5(a). The corresponding $S(k)$ in Fig. 5(b) contains a series of peaks that reflect the ordered nature of the state, which resembles the zig-zag state in Fig. 1(e,f) except that the system is more ordered and the zig-zag structure is wider. For $F_p = 0.1$ the zig-zag state transitions into a hexagonal lattice and the peak in F_c begins to disappear. Some experiments examining vortices in q1D periodic pinning structures show that peaks in the critical current occur at certain fillings[49,51-53] in regimes where the pinning is weak, whereas other experiments performed in the strong pinning limit reveal more step-like features in the critical current. This suggests that the experiments in the strong pinning limit are producing buckling transitions[54].

In Fig. 6 we plot representative real space images with the matching $S(k)$ for some other substrate strengths to highlight other types of ordering we observe. Figure 6(a) shows the real space ordering of the vortices at $F_p = 0.5$ and $w/a = 4.825$, where the vortex lattice is polycrystalline and contains regions of triangular ordering with different orientations. The corresponding structure factor in Fig. 6(b) has ring features with some remnant of the smectic ordering appearing at smaller values of k. In Fig. 6(c), at $F_p = 2.0$ and $w/a = 4.33$ an r_4 state appears, while $S(k)$ in Fig. 6(d) has smectic ordering features along with additional crystalline ordering signatures due to the ordered arrangement of the particles within the troughs. At $F_p = 2.0$ and $w/a = 4.67$ in Fig. 6(e), a new type of ordered structure appears in which the vortices can pack more closely by forming alternate regions of r_3 and r_4 states, producing a considerable amount of triangular ordering as seen in the plot of $S(k)$ in Fig. 6(f), where there are sixfold peaks at large k and smectic peaks at smaller k. In Figs. 6(g,h), for $F_p = 2.0$ and $w/a = 5.15$, a more disordered structure appears, with some regions of the sample containing r_4 or r_5 states.

IV. LATTICE ROTATIONS FOR WEAK SUBSTRATES

We have also studied systems with a pinning strength of $F_p = 0.02$. Here, for $w/a > 1.77$ the vortices form a triangular lattice and the features associated with the buckling transitions observed in Fig. 3 are lost. In this case the vortex lattice can orient at various angles with respect to the underlying substrate. In Fig. 7(a) we show
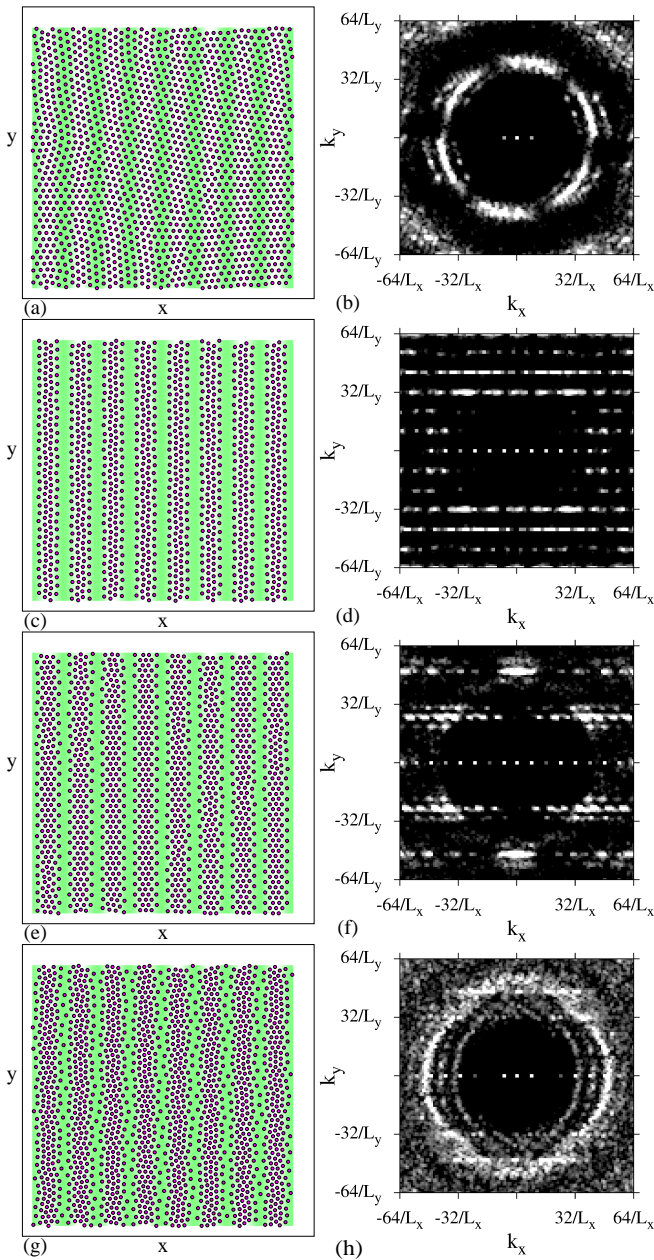
FIG. 6: Real space images (left column), with the substrate minima indicated by lighter regions and the vortex positions marked with circles, and $S(k)$ (right column). (a,b) At $F_p = 0.5$ and $w/a = 4.825$ there is a polycrystalline structure. (c,d) At $F_p = 2.0$ and $w/a = 4.33$ there is a partially ordered r_4 structure. (e,f) At $F_p = 2.0$ and $w/a = 4.67$, an ordered structure appears. (g,h) At $F_p = 2.0$ and $w/a = 5.15$ the structure is disordered.

the real space vortex positions at $w/a = 2.8$, where the vortices form a triangular lattice that is aligned at an angle $\theta = 27.6°$ with respect to the y-axis. In Fig. 7(b) at $w/a = 3.272$, $\theta = 24°$, while in Fig. 7(c) at $w/a = 3.53$, $\theta = 2.9°$, and in Fig. 7(d) at $w/a = 3.75$, $\theta = 13.2°$. In Ref.[80], Guillamon et $al.$ observed experimentally that vortices on a q1D substrate retained triangular order-
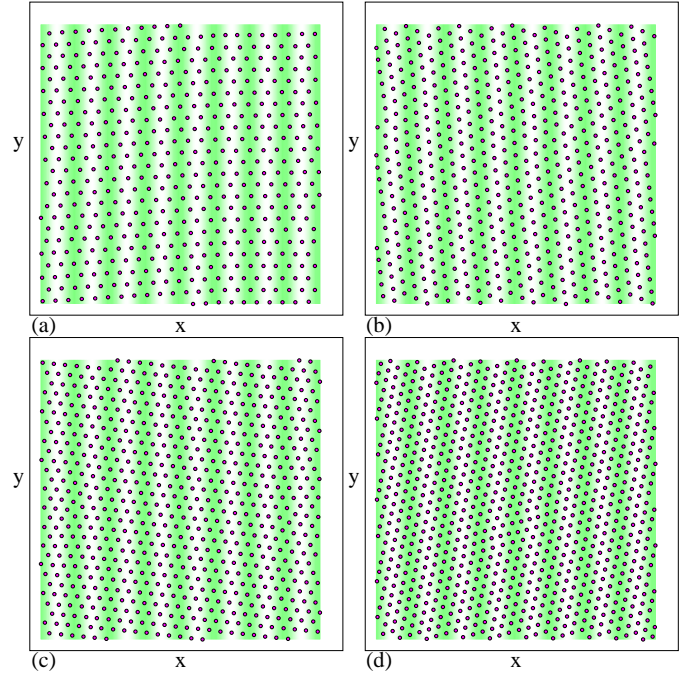
FIG. 7: Real space images of the vortices in a sample with $F_p = 0.02$ showing that the hexagonal vortex lattice can adopt various orientations θ with respect to the substrate. (a) At $w/a = 2.8$, $\theta = 27.6°$. (b) At $w/a = 3.272$, $\theta = 24°$. (c) At $w/a = 3.53$, $\theta = 2.9°$. (d) At $w/a = 3.75$, $\theta = 13.2°$.

ing but that the vortex lattice was oriented at an angle θ ranging from $\theta = 0$ to $\theta = 30°$ with respect to the substrate. In several cases, they found that the system locked to specific angles close to $\theta = 30°$, $\theta = 24°$, and $\theta = 0°$. We find a much larger variation in the orientation of the lattice with respect to the substrate as a function of filling than was observed in the experiments, which may be due to differences the pinning strength or the finite size of our simulations. Our results show that for weak pinning, the buckling transitions are lost and are replaced with orientational transitions of the vortex lattice with respect to the substrate. Another feature we observe when the pinning strength is increased is that the vortex lattice becomes disordered or polycrystalline. Guillamon et $al.$ also observe that at higher fillings the vortex lattice becomes disordered; however, in their system there are strong random vortex density fluctuations, while for our thermally annealed samples the vortex density at higher fields is generally uniform.

V. DYNAMIC PHASES

In Fig. 8 we plot simultaneously P_6 and the average nearest neighbor spacing $\bar{d}_{nn}$ versus F_d for a sample with $F_p = 1.5$ at varied w/a. Here, we obtain $\bar{d}_{nn}$ by performing a Voronoi tesselation to identify the z_i nearest neighbors of particle i, and then take $\bar{d}_{nn} =$

FIG. 8: The fraction of six-fold coordinated vortices P_6 (dark blue curves) and the average nearest-neighbor distance $\bar{d}_{nn}$ (light red curves) vs F_d for a system with $F_p = 1.5$. (a) At $w/a = 1.767$ the system depins from an r_1 state. (b) At $w/a = 2.5$ the system dynamically orders into a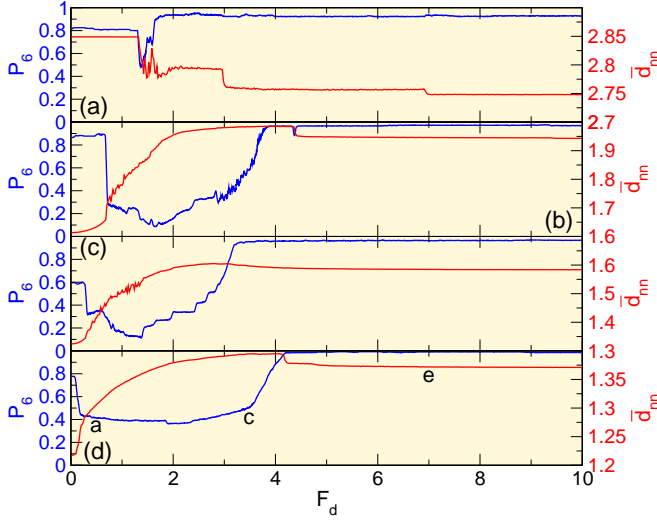 moving triangular lattice with $P_6 = 0.97$. (c) $w/a = 3.061$. (d) At $w/a = 3.535$, the onset of the dynamically ordered phase coincides with a drop in $\bar{d}_{nn}$ near $F_d = 4.0$. The labels a, c, and e correspond to the values of F_d used for the images in Fig. 9.

$(N \sum_i z_i)^{-1} \sum_{i=1}^{N} \sum_{j=1}^{z_i} r_{ij}$, where r_{ij} is the distance between particle i and its jth nearest neighbor. For $w/a = 1.767$ in Fig. 8(a), $P_6 = 0.83$ in the pinned r_1 state that occurs for $0 < F_d < 1.4$. There is a dip in P_6 over the range $1.4 < F_d < 1.7$, corresponding to the plastic flow state in which some of the vortices remain immobile while other vortices hop in and out of the potential wells. For $F_d > 1.7$, P_6 increases and reaches a saturated value of $P_6 = 0.93$ when the vortices form a moving triangular lattice containing a small fraction of dislocations. The value of $\bar{d}_{nn}$ drops at the depinning transition, and several additional drops in $\bar{d}_{nn}$ occur at higher drives. In the r_1 pinned state, each vortex has two close nearest neighbors that are in the same pinning trough, and four more distant nearest neighbors that are in adjacent pinning troughs. Once the vortices depin and enter a moving state, they adopt a more isotropic structure, causing $\bar{d}_{nn}$ to drop as the distance to the four more distant nearest neighbors decreases. The additional drops in $\bar{d}_{nn}$ at higher F_d occur whenever the vortex lattice rearranges to become still more isotropic.

In Fig. 8(b) we plot P_6 and $\bar{d}_{nn}$ versus F_d for the same sample at $w/a = 2.5$ where an ordered zig-zag state with $P_6 = 0.89$ appears at zero drive, similar to that shown in Fig. 1(e). The depinning threshold is $F_c = 0.65$, much lower than the value of F_c for the $w/a = 1.767$ filling in Fig. 8(a), and the depinning transition is marked by a drop in P_6 to $P_6 = 0.2$. Over the range $0.65 < F_d \lesssim 2.0$, the vortices are in a dynamically disordered state, while

FIG. 9: Real space images (left column), with the substrate minima indicated by lighter regions and the vortex positions marked with circles, and $S(k)$ (right column) for the dynamic system from Fig. 8(d) with $F_p = 1.5$ and $w/a = 3.535$ at the values of F_d labeled a, c, and e. (a,b) At $F_d = 0.5$ the sample contains pinned vortices coexisting with individual vortices that hop from trough to trough. (c,d) At $F_d = 3.5$, all the vortices move together to form a disordered lattice with a periodic density modulations. (e,f) At $F_d = 7.0$ the system forms a moving floating triangular lattice.

the saturation of $\bar{d}_{nn}$ above $F_d \approx 2.0$ indicates that a partially ordered state has formed. The value of P_6 does not reach a maximum until $F_d = 3.9$, where $P_6 \approx 0.97$ and an ordered state appears. For $1.5 < F_d < 3.9$, we observe a moving density-modulated solid. The value of F_c^{tr}, the drive at which the sample reaches a moving triangular lattice state, is higher for $w/a = 2.5$ than for $w/a = 1.767$, even though the depinning threshold F_c is smaller for the $w/a = 2.5$ system. At $w/a = 2.5$, $\bar{d}_{nn}$ is initially small and jumps up at the depinning transition, unlike the decrease in $\bar{d}_{nn}$ at depinning found in Fig 8(a). Since the vortices in Fig. 8(b) form a zig-zag r_2 structure in the pinned state, each vortex has four close
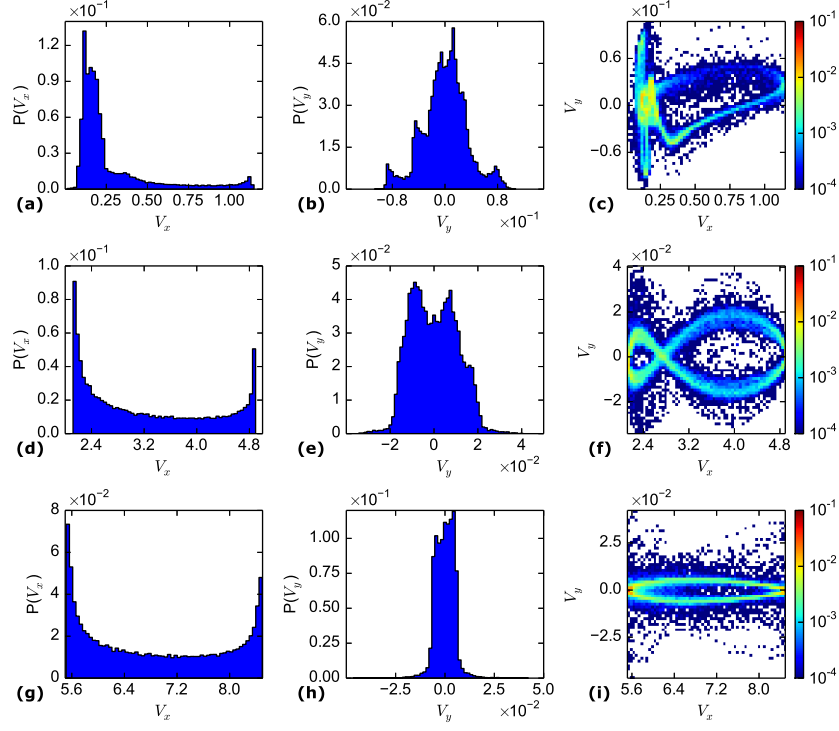
FIG. 10: Vortex velocities for the system in Fig. 9 with $F_p = 1.5$ and $w/a = 3.535$. Left column: Histogram $P(V_x)$ of the instantaneous vortex velocities in the driving direction V_x. Center column: Histogram $P(V_y)$ of the instantaneous vortex velocities in the transverse direction V_y. Right column: Heightfield map of V_y versus V_x. (a,b,c) The plastic flow regime at $F_d = 0.5$. (d,e,f) The moving modulated solid regime at $F_d = 3.5$. (g,h,i) The moving floating solid regime at $F_d = 7.0$.

nearest neighbors in the same pinning trough, and two more distant nearest neighbors in an adjacent pinning trough. This causes $\bar{d}_{nn}$ to be smaller in the pinned state than it was for the r_1 structure in Fig. 8(a), and when the vortex lattice becomes more isotropic in the moving state, $\bar{d}_{nn}$ increases rather than decreasing as the two halves of each zig-zag structure move further apart. At $F_d = 4.1$ we observe a drop in $\bar{d}_{nn}$ that coincides with a dip in P_6. This feature is associated with a transition from a density-modulated lattice to a more uniform moving floating lattice.

In Fig. 8(c), we show P_6 and $\bar{d}_{nn}$ versus F_d at $w/a = 3.061$ where there is an r_3 pinned state, similar to that illustrated in Fig. 2(a). Here the depinning threshold $F_c = 0.3$, and the system transitions into a moving triangular lattice at $F_c^{\mathrm{tr}} = 1.6$, which is somewhat lower than the value of F_c^{tr} for $w/a = 2.5$ in Fig. 8(b). The behavior of $\bar{d}_{nn}$ in Fig. 8(c) follows a similar pattern as in Fig. 8(b), with $\bar{d}_{nn}$ increasing with increasing F_d. We plot the same quantities for $w/a = 3.535$ in Fig. 8(d), where the depinning threshold $F_c \approx 0.087$ and the system dynamically orders for $F_d > 4.0$. There is a small dip in $\bar{d}_{nn}$ at $F_d = 4.15$ along with a saturation in P_6 which is correlated with a structural change to a dynamic floating lattice.

In order to characterize the nature of the dynamic vor-

tex structures in the moving states, in Fig. 9(a,b) we plot the real space images and $S(k)$ for the system in Fig. 8(d) at $w/a = 3.535$ and $F_d = 0.5$. Here, individual vortices jump from one pinning well to the next while a portion of the vortices remain immobile in the substrate minima. As shown in the plot of $S(k)$, the vortex configuration is fairly ordered and takes the form of a distorted non-triangular structure which causes P_6 to be low for this value of F_d. For $F_d > F_p$, the vortices move together so there is no plastic motion, and form a distorted lattice containing pronounced density modulations as shown in Fig. 9(c,d) for $F_d = 3.5$. For $F_d > 4.0$ we find a transition from the density modulated lattice to a moving homogeneous floating triangular lattice which coincides with the drop in $\bar{d}_{nn}$ in Fig. 8(d) and the maximum in P_6. Fig. 9(e) shows the floating lattice at $F_d = 7.0$, where as indicated in Fig. 9(f) $S(k)$ contains sixfold peaks that are indicative of triangular ordering. The smectic ordering induced by the substrate is substantially weaker or almost absent at this drive, as shown by the weakness of the spots in $S(k)$ at $k_y = 0$, indicating that the system has formed a floating solid. We find similar types of transitions in the dynamics at other fillings as well.

We can also characterize the different dynamic states in Figs. 8 and 9 by examining histograms of the vortex velocities. In Fig. 10(a) we plot the distribution $P(V_x)$ of
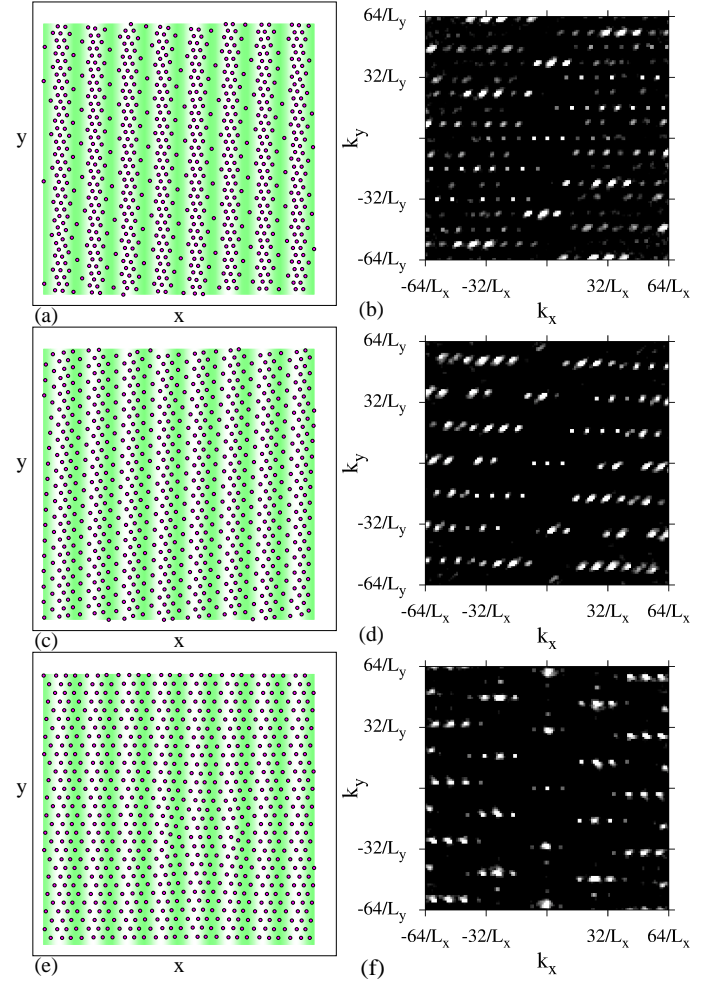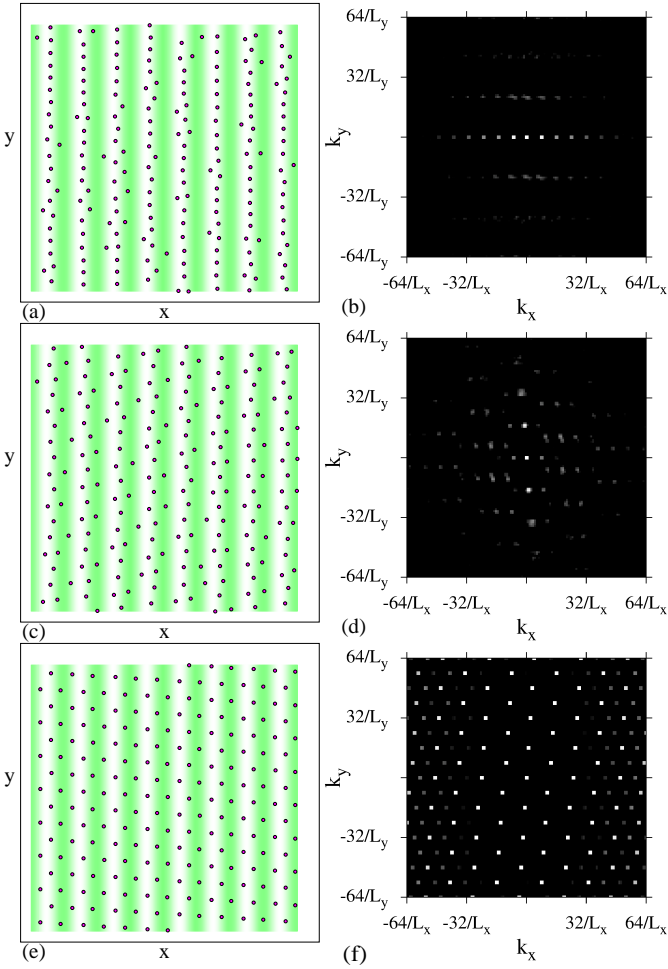
FIG. 11: Real space images (left column), with the substrate minima indicated by lighter regions and the vortex positions marked with circles, and $S(k)$ (right column) for a system with $F_p = 0.5$ and $w/a = 1.767$. (a,b) The plastic flow phase at $F_d = 0.3$ where there is individual vortex hopping from well to well. The $S(k)$ peaks indicate a smectic phase with periodic ordering along the $x-$direction. (c,d) At $F_d = 0.6$, all the vortices are flowing and form chains that are aligned in the x-direction. $S(k)$ shows that a new smectic order has appeared with periodic ordering along the y-direction. (e,f) At $F_d = 3.6$ there is a moving floating triangular crystal.

V_x in the driving direction at $F_d = 0.5$ for the system in Fig. 9(a,b) with $F_p = 1.5$ and $w/a = 3.535$. Figure 10(b) shows the transverse velocities $P(V_y)$, while in Fig. 10(c) we plot V_y versus V_x as a heightfield map. At this drive, the motion is plastic and occurs by individual vortex hopping, so there is a sharp peak in $P(V_x)$ at $V_x = 0.15$ which reflects the fact that most of the vortices are slowly moving within an individual pinning trough. When a single vortex jumps into an adjacent pinning trough, it creates a pulse of motion through the trapped vortices that triggers the jump of another single vortex to the next pinning trough, where the process repeats. This depinning cycle creates two peaks in $P(V_x)$. The peak at low V_x cor-

responds to the motion of a velocity pulse through the dense assembly of vortices at the bottom of the pinning trough, while the peak at high V_x is produced by individual vortices escaping over the potential maximum. This peak falls near $V_x = 1.1$, which is larger than F_d, reflecting the fact that after an individual vortex passes the crest of the substrate maximum, the substrate contributes an additional force term in the driving direction as the vortex moves toward the next substrate minimum. In this case the maximum force exerted by the pinning site is $F_p = 1.5$ while the driving force is $F_d = 0.5$, so that the maximum possible instantaneous vortex velocity would be $V_x = 2.0$; however, vortex-vortex interactions prevent individual vortices from moving this rapidly. In Fig. 10(b), $P(V_y)$ is centered at $V_y = 0$ since there is no driving force in the transverse direction; however, we observe some asymmetry in $P(V_y)$ as well as peaks at finite V_y due to the fact that the vortex lattice segments inside the pinning troughs are oriented at an angle with respect to the substrate symmetry direction, as shown in Fig. 9(a). This asymmetry also appears in the V_y versus V_x plot in Fig. 10(c), which has two prominent features. The first is a wide band of V_y values at low V_x that are associated with soliton-like pulses moving through the dense regions of the vortex clusters, which push vortices in both the positive and negative y-direction. The second is the loop shape at larger V_x values which corresponds to motion in which the vortices are accelerated or decelerated as they pass over the substrate maxima and minima.

In Fig. 10(d,e,f) we show instantaneous velocity plots for the system in Fig. 9(c,d) with $F_d = 3.5$ where the vortices are moving elastically in the density-modulated solid phase. Here $P(V_x)$ in Fig. 10(d) has peaks at $V_x = 2.01$ and $V_x = 4.75$ which are smoothly connected by finite $P(V_x)$ values. The shape of this histogram shows the velocity imposed by the driving force of $F_d = 3.5$ when the substrate forces alternately act with or against the driving force. When the substrate force is against the drive the velocity is $V_x = F_d - F_p = 2.0$, while when the substrate and driving forces are in the same direction, $V_x = F_d + F_p = 5.0$, close to the observed values of the peaks in $P(V_x)$. In Fig. 10(e), $P(V_y)$ has two peaks close to $V_y = 0.1$ and $V_y = -0.1$, indicating that there is an oscillatory motion in the y-direction. This effect can be seen more clearly in the V_y versus V_x plot in Fig. 10(f) which has two symmetric lobes. Since the vortices are in a density-modulated lattice, shearing in the y-direction occurs between adjacent density modulations, with one density modulation moving in the positive y-direction while the other moves in the negative y-direction.

The velocity plots for the system in Fig. 9(e,f) at $F_d = 7.0$ appear in Fig. 10(g,h,i). In Fig. 10(g), $P(V_x)$ has a two-peak feature similar to that in Fig. 10(d), but with peak values at $V_x = 5.52$ and $V_x = 8.4$. Figure 10(h) shows that $P(V_y)$ has a single peak centered at $V_y = 0$, while in Fig. 10(i), there is a single lobe in the
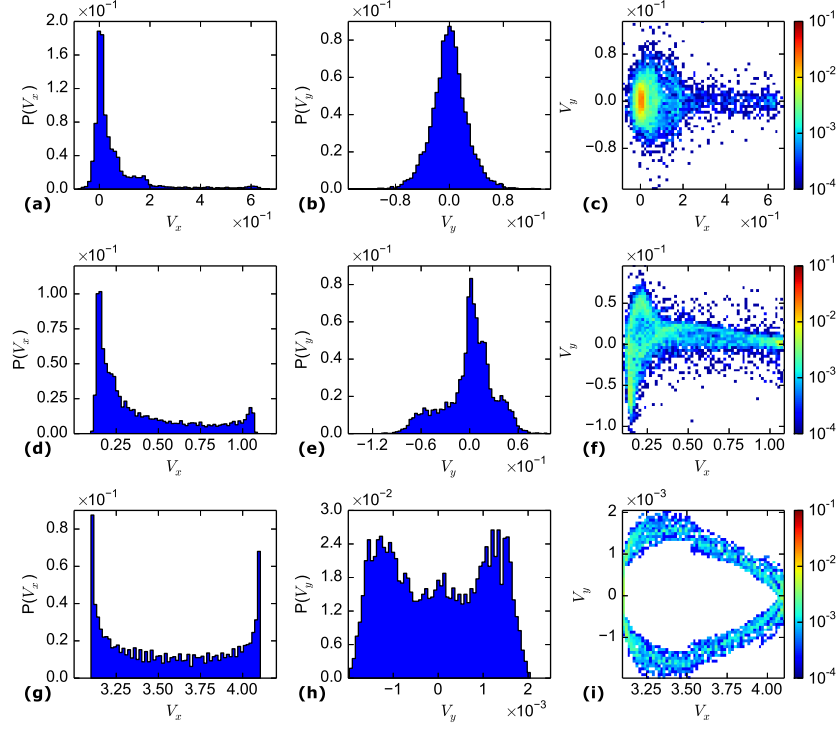
FIG. 12: Vortex velocities for the system in Fig. 11 with $F_p = 0.5$ and $w/a = 1.767$. Left column: $P(V_x)$. Center column: $P(V_y)$. Right column: Heightfield map of V_y versus V_x. (a,b,c) The plastic flow phase at $F_d = 0.3$ where there is a large peak in $P(V_x)$ at $V_x = 0$ due to the pinned vortices. (d,e,f) The moving smectic phase from Fig. 11(c,d) at $F_d = 0.6$. (g,h,i) The moving triangular solid phase at $F_d = 3.6$.

V_y versus V_x plot. Here the vortices have formed a floating triangular solid, and their motion is close to one-dimensional along the driving direction. As F_d is further increased, the width of the lobe feature in the V_y direction gradually decreases. We find similar histograms for the other fillings in the strong pinning limit for the plastic flow, moving modulated solid, and moving floating solid regimes.

A. Smectic to Smectic Transitions

For $F_p < 1.0$, we find that a dynamically induced smectic to smectic transition can occur. In Fig. 11(a,b) we show the real space and $S(k)$ images for a system with $F_p = 0.5$ and $w/a = 1.767$ in the plastic flow regime where there is a combination of vortices that are trapped in the pinning troughs and a smaller amount of vortices that hop by jumping from one trough to the next and then triggering a jump of another vortex from one trough to the next. Here, $S(k)$ indicates that the overall system has smectic ordering due to the chain-like structure of the vortices within the pinning troughs. In Fig. 12(a) we plot $P(V_x)$ at $F_d = 0.3$, where there is a peak at $V_x = 0$ due to the pinned vortices along with a small bump at $V_x = 0.6$ due to the vortex hopping. Figure 12(b) shows

that $P(V_y)$ has a maximum at $V_y = 0$, while in Fig. 12(c), the V_y versus V_x plot is asymmetric in V_y, with a peak at $V_x = V_y = 0.0$ and a second peak at higher V_x produced by the moving vortices.

In Fig. 11(c) we show the real space vortex configuration at $F_d = 0.6$, which is higher than the maximum pinning force of $F_p = 0.5$. All the vortices are in motion, but instead of retaining their alignment along the y-direction induced by the substrate, they form a chain-like structure aligned in the x-direction with a slight tilt in the positive y-direction. This alignment in the drive direction is more clearly seen in the corresponding $S(k)$ in Fig. 11(d), where the peaks fall along $k_x = 0$, indicating a smectic phase with ordering along the y-direction. There are some very weak peaks on the $k_y = 0$ axis due to the substrate, but overall the vortex structure is a smectic state rotated 90° from the y-axis. The peaks do not fall exactly at $k_x = 0$ but are at a slight angle, due to the channels in Fig. 11(c) being slightly tilted in the positive y-direction. In Fig. 12(d), $P(V_x)$ for this case shows a peak at $V_x = 0.19$, while there is an absence of weight in $P(V_x)$ at $V_x = 0.0$, indicating that the vortices are always in motion. Figure 12(e) shows that $P(V_y)$ peaks at $V_y = 0.0$ and has an overall asymmetry, which also appears in the V_y versus V_x plot in Fig. 12(f). The vortex channeling occurs when the vortices form effective pairs
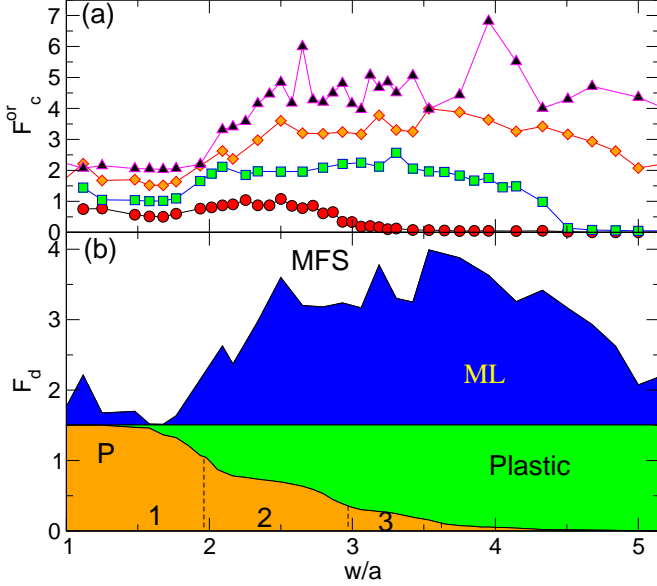
FIG. 13: (a) F_c^{or}, the drive at which the system transitions from a density modulated moving crystal to an ordered moving floating solid, vs w/a at $F_p = 0.5$ (red circles), 1.0 (green squares), 1.5 (orange diamonds), and 2.0 (black triangles). (b) Dynamic phase diagram as a function of F_d and w/a for a system with $F_p = 1.5$. P: pinned phase. Plastic: plastic flow regime. ML: moving modulated lattice state. MFS: moving flowing solid state. Dashed lines are guides to the eye that indicate the transition from r_1 to r_2, r_2 to r_3, and r_3 to a disordered pinned state.

aligned along the x-direction. In each pair, one vortex is slowed by the backward-sloping side of the potential trough, while the other vortex is sped up by the forward-sloping side of the potential. The faster vortex pushes the slower vortex, giving the pair an increased net motion along the x direction. This pairing effect is visible in the real space image in Fig. 11(c).

As F_d further increases, there is a transition to a flowing solid phase as shown in Fig. 11(e,f) for $F_d = 3.6$, where $S(k)$ has sixfold ordering. The corresponding $P(V_x)$ in Fig. 12(g) has two peaks, while $P(V_y)$ in Fig. 12(h) has a symmetrical distribution with three peaks indicating that there is an oscillation in the vortex orbits in the y-direction. The plot of V_y versus V_x in Fig. 12(h) contains a single lobe similar to that found for the moving floating solid in Fig. 10(i). As F_d is increased still further, the width of this lobe in the V_y direction decreases. The smectic-to-smectic transition is limited to the range $1.5 < w/a < 2$, in which two vortices can fit between adjacent potential maxima in the dynamically moving regime.

VI. DYNAMICAL PHASE DIAGRAM

For $F_p > 0.25$, the drive F_c^{or} at which the system transitions from a density modulated moving crystal to an ordered moving floating solid shows considerable variation with w/a, particularly for the larger values of F_p. In Fig. 13(a) we plot F_c^{or}, determined from the location of a feature in P_6, versus w/a for $F_p = 0.5$, 1.0, 1.5, and 2.0. For $F_p = 0.5$, F_c^{or} has a local maximum near $w/a = 2.5$, and then drops for $w/a > 3.0$. In the pinned phase for $w/a > 3.0$, the system forms a polycrystalline state, and in the moving state the grains realign to form a moving crystalline state. For $F_p = 1.0$, 1.5, and 2.0, when $w/a < 1.75$ the system depins from a single chain of vortices and can partially form a moving crystal state. When w/a is large enough that a pinned zig-zag state forms, the moving density-modulated state can persist up to much higher drives. For $F_p = 1.0$ the system forms a pinned polycrystalline state for $w/a > 4.5$ which coincides with the drop in F_c^{or} for $w/a > 4.5$. For $F_p = 1.5$ and 2.0, there are local peaks in F_c^{or} that correlate with the moving buckled phases which occur when groups of vortices can fit between adjacent pinning maxima as the vortices move. This effect is most pronounced for $F_p = 2.0$.

In Fig. 13(b) we plot a dynamic phase diagram as a function of F_d and w/a for a system with $F_p = 1.5$. Above depinning in the regime where $F_d < F_p$, the system is in a plastic flow state in which there is a coexistence of moving vortices and immobile vortices. In this regime the structure factor generally shows disordered features. For $F_d > F_p$, all the vortices are moving and the system is either in a modulated lattice (ML) state or a moving flowing solid (MFS) state. We find similar dynamical phase diagrams for other values of $F_p > 1.0$, while for the weaker substrates, the size of the plastic flow region is reduced and the ML phase is replaced with a smectic moving state similar to that shown in Fig. 11(c,d).

VII. DISCUSSION

The dynamic phases we observe have certain similarities to the dynamic states observed for vortices moving over random pinning arrays in that there can be pinned, plastic, and dynamically ordered phases as a function of external drive[81–86]. There are some differences, including the fact that the moving modulated lattice we observe does not form a smectic state that is aligned in the drive direction, as found for vortices moving over random pinning arrays[83–86]. Future studies might consider combinations of random disorder with periodic disorder, which would introduce a competition in the moving phase between the smectic ordering imposed by the substrate and the smectic ordering induced by the drive. Additionally, for random pinning arrays simulations indicate that for increasing vortex density, the drive at which the transition to the ordered state occurs decreases

due to the increase in the strength of the vortex-vortex interactions[86]. For the q1D substrate, the location of the ordering transition shows strong fluctuations due to the ability of the moving lattice to become dynamically commensurate with the periodicity of the substrate.

VIII. SUMMARY

We examine the statics and dynamics of vortices interacting with a periodic quasi-one-dimensional substrate in the limit where the vortex lattice spacing is smaller than the spacing of the periodic lattice. For weak substrate strengths, we find that the vortices retain hexagonal ordering but exhibit numerous rotations with respect to the substrate, similar to recent experimental observations. For stronger substrates there are a series of buckling transitions where the vortices can form anisotropic 1D chains, zig-zag patterns, and higher order numbers of chains within each substrate minimum. At some fillings the overall lattice has long range order and becomes partially distorted at the transitions between these states. For higher fillings the buckling transitions are lost and the system forms a polycrystalline state. We also find that the depinning shows a series of step like features when the system transitions from a state with n chains to a state with $n+1$ chains in each substrate minimum, and that for weaker pinning there are some cases where there is a peak in the depinning force as a function of filling. For weak substrates, under an applied drive the vortices depin elastically and retain their triangular ordering, while for strong substrates the buckled states transition to a partially disordered flowing state followed by various other transitions into moving modulated crystal or homogeneous floating moving crystal states. Our results should also be applicable to other systems of particles with repulsive interactions in the presence of a periodic quasi-one dimensional substrate, such as electron crystals, colloids, and ions in optical traps.

[1] P. Bak, Commensurate phases, incommensurate phases and the devil's staircase, Rep. Prog. Phys. **45**, 587 (1982).

[2] O.M. Braun and Y.S. Kivshar, *The Frenkel-Kontorova Model: Concepts, Methods, and Applications* (Springer-Verlag, Berlin, 2004).

[3] A.D. Novaco and J.P. McTague, Orientational epitaxy the orientational ordering of incommensurate structures, Phys. Rev. Lett. **38**, 1286 (1977).

[4] S.N. Coppersmith, D.S. Fisher, B.I. Halperin, P.A. Lee, and W.F. Brinkman, Dislocations and the commensurate-incommensurate transition in two dimensions, Phys. Rev. B **25**, 349 (1982).

[5] M. Peyrard and S. Aubry, Critical behaviour at the transition by breaking of analyticity in the discrete Frenkel–Kontorova model, J. Phys. C: Solid State Phys. **16**, 1593 (1983).

[6] S. Bleil, H.H. von Grunberg, J. Dobnikar, R. Castaneda-Priego, and C. Bechinger, Strain-induced domain formation in two-dimensional colloidal systems, Europhys. Lett. **73**, 450 (2006).

[7] T. Bohlein, J. Mikhael, and C. Bechinger, Observation of kinks and antikinks in colloidal monolayers driven across ordered surfaces, Nature Mater. **11**, 126 (2012).

[8] A. Vanossi, N. Manini, and E. Tosatti, Static and dynamic friction in sliding colloidal monolayers, Proc. Natl. Acad. Sci. (USA) **109**, 16429 (2012).

[9] J. Tekic, O.M. Braun, and B.B. Hu, Dynamic phases in the two-dimensional underdamped driven Frenkel-Kontorova model, Phys. Rev. E **71**, 026104 (2005).

[10] A. Vanossi, N. Manini, M. Urbakh, S. Zapperi, and E. Tosatti, Modeling friction: From nanoscale to mesoscale, Rev. Mod. Phys. **85**, 529 (2013).

[11] D. Mandelli, A. Vanossi, N. Manini, and E. Tosatti, Friction boosted by equilibrium misalignment of incommensurate two-dimensional colloid monolayers, Phys. Rev. Lett. **114**, 108302 (2015).

[12] M. Baert, V.V. Metlushko, R. Jonckheere, V.V. Moshchalkov, and Y. Bruynseraede, Composite flux-line lattices stabilized in superconducting films by a regular array of artificial defects, Phys. Rev. Lett. **74**, 3269 (1995).

[13] K. Harada, O. Kamimura, H. Kasai, T. Matsuda, A. Tonomura, and V.V. Moshchalkov, Direct observation of vortex dynamics in superconducting films with regular arrays of defects, Science **274**, 1167 (1996).

[14] J.I. Martín, M. Vélez, J. Nogués, and I.K. Schuller, Flux pinning in a superconductor by an array of submicrometer magnetic dots, Phys. Rev. Lett. **79**, 1929 (1997).

[15] D.J. Morgan and J.B. Ketterson, Asymmetric flux pinning in a regular array of magnetic dipoles, Phys. Rev. Lett. **80**, 3614 (1998).

[16] C. Reichhardt, C. J. Olson, and F. Nori, Commensurate and incommensurate vortex states in superconductors with periodic pinning arrays, Phys. Rev. B **57**, 7937 (1998).

[17] C. Reichhardt and C. J. Olson Reichhardt, Vortex molecular crystal and vortex plastic crystal states in honeycomb and kagome pinning arrays, Phys. Rev. B **58**, 064523 (2007).

[18] U. Welp, Z.L. Xiao, V. Novosad, and V.K. Vlasko-Vlasov, Commensurability and strong vortex pinning in nanopatterned Nb films, Phys. Rev. B **71**, 014505 (2005).

[19] G.R. Berdiyorov, M.V. Milosevic, and F.M. Peeters, Novel commensurability effects in superconducting films with antidot arrays, Phys. Rev. Lett. **96**, 207001 (2006).

[20] S. Goldberg, Y. Segev, Y. Myasoedov, I. Gutman, N.

Avraham, M. Rappaport, E. Zeldov, T. Tamegai, C.W. Hicks, and K.A. Moler, Mott insulator phases and first-order melting in $Bi_2Sr_2CaCu_2O_{8+\delta}$ crystals with periodic surface holes, Phys. Rev. B **79**, 064523 (2009).

[21] I. Swiecicki, C. Ulysse, T. Wolf, R. Bernard, N. Bergeal, J. Briatico, G. Faini, J. Lesueur, and J.E. Villegas, Strong field-matching effects in superconducting $YBa_2Cu_3O_{7\delta}$ films with vortex energy landscapes engineered via masked ion irradiation, Phys. Rev. B **85**, 224502 (2012).

[22] T.C. Halsey, Josephson-junction arrays in transverse magnetic fields: Ground states and critical currents, Phys. Rev. B **31**, 5728 (1985).

[23] H.D. Hallen, R. Seshadri, A.M. Chang, R.E. Miller, L.N. Pfeiffer, K.W. West, C.A. Murray, and H.F. Hess, Direct spatial imaging of vortices in a superconducting wire network, Phys. Rev. Lett. **71**, 3007 (1993).

[24] J.W. Reijnders and R.A. Duine, Pinning of vortices in a Bose-Einstein condensate by an optical lattice, Phys. Rev. Lett. **93**, 060401 (2004).

[25] H. Pu, L.O. Baksmaty, S. Yi, and N.P. Bigelow, Structural phase transitions of vortex matter in an optical lattice, Phys. Rev. Lett. **94**, 190401 (2005).

[26] S. Tung, V. Schweikhard, and E. A. Cornell, Observation of vortex pinning in Bose-Einstein condensates, Phys. Rev. Lett. **97**, 240402 (2006).

[27] H.P. Büchler, G. Blatter, and W. Zwerger, Commensurate-incommensurate transition of cold atoms in an optical lattice, Phys. Rev. Lett. **90**, 130401 (2003).

[28] B. Gränz, S.E. Korshunov, V.B. Geshkenbein, and G. Blatter, Competing structures in two-dimensional trapped dipolar gases, Phys. Rev. B **90**, 060101 (2014).

[29] A. Benassi, A. Vanossi, and E. Tosatti, Nanofriction in cold ion traps, Nature Commun. **2**, 236 (2011).

[30] A. Bylinskii, D. Gangloff, and V. Vuletic, Tuning friction atom-by-atom in an ion-crystal simulator, Science **348**, 6239 (2015).

[31] K. Mangold, P. Leiderer, and C. Bechinger, Phase transitions of colloidal monolayers in periodic pinning arrays, Phys. Rev. Lett. **90**, 158302 (2003).

[32] S. El Shawish, J. Dobnikar, and E. Trizac, Colloidal ionic complexes on periodic substrates: Ground-state configurations and pattern switching, Phys. Rev. E **83**, 041403 (2011).

[33] D. McDermott, J. Amelang, L.M. Lopatina, C.J. Olson Reichhardt, and C. Reichhardt, Domain and stripe formation between hexagonal and square ordered fillings of colloids on periodic pinning substrates, Soft Matter **9**, 4607 (2013).

[34] T. Neuhaus, M. Marechal, M. Schmiedeberg, and H. Löwen, Rhombic preordering on a square substrate, Phys. Rev. Lett. **110**, 118301 (2013).

[35] J. Mikhael, J. Roth, L. Helden, and C. Bechinger, Archimedean-like tiling on decagonal quasicrystalline surfaces, Nature **454**, 501 (2008).

[36] J. Mikhael, G. Gera, T. Bohlein, and C. Bechinger, Phase behavior of colloidal monolayers on quasiperiodic substrates, Soft Matter **7**, 1352 (2011).

[37] S. Field, S. James, J. Barentine, V. Metlushko, G. Crabtree, H. Shtrikman, B. Ilic, and S. Brueck, Vortex configurations, matching, and domain structure in large arrays of artificial pinning centers, Phys. Rev. Lett. **88**, 067003 (2002).

[38] A.N. Grigorenko, S.J. Bending, M.J. Van Bael, M. Lange, V.V. Moshchalkov, H. Fangohr, and P.A.J. de Groot, Symmetry locking and commensurate vortex domain formation

in periodic pinning arrays, Phys. Rev. Lett. **90**, 237001 (2003).

[39] M. Baert, V.V. Metlushko, R. Jonckheere, V.V. Moshchalkov, and Y. Bruynseraede, Flux phases and quantized pinning force in superconductor with a periodic lattice of pinning centres, Europhys. Lett. **29**, 157 (1995).

[40] C. Reichhardt and N. Grønbech-Jensen, Critical currents and vortex states at fractional matching fields in superconductors with periodic pinning, Phys. Rev. B **63**, 054510 (2001).

[41] D. McDermott, J. Amelang, C.J. Olson Reichhardt, and C. Reichhardt, Dynamic regimes for driven colloidal particles on a periodic substrate at commensurate and incommensurate fillings, Phys. Rev. E **88**, 062301 (2013).

[42] A. Chowdhury, B.J. Ackerson, and N.A. Clark, Laser-induced freezing, Phys. Rev. Lett. **55**, 833 (1985).

[43] J. Chakrabarti, H.R. Krishnamurthy, A.K. Sood, and S. Sengupta, Reentrant melting in laser field modulated colloidal suspensions, Phys. Rev. Lett. **75**, 2232 (1995).

[44] J. Hu and R.M. Westervelt, Commensurate-incommensurate transitions in magnetic bubble arrays with periodic line pinning, Phys. Rev. B **55**, 771 (1997).

[45] Q.-H. Wei, C. Bechinger, D. Rudhardt, and P. Leiderer, Experimental study of laser-induced melting in two-dimensional colloids, Phys. Rev. Lett. **81**, 2606 (1998).

[46] E. Frey, D. Nelson, and L. Radzihovsky, Light-induced melting of colloidal crystals in two dimensions, Phys. Rev. Lett. **83**, 2977 (1999).

[47] C. Richter, M. Schmiedeberg, and H. Stark, A colloidal model system with tunable disorder: Solid-fluid transition and discontinuities in the limit of zero disorder, Eur. Phys. J. E **34**, 107 (2011).

[48] L. Zaidouny, T. Bohlein, R. Roth, and C. Bechinger, Light-induced phase transitions of colloidal monolayers with crystalline order, Soft Matter **9**, 9230 (2013).

[49] O. Daldini, P. Martinoli, J. L. Olsen, and G. Berner, Vortex-line pinning by thickness modulation of superconducting films, Phys. Rev. Lett. **32**, 218 (1974).

[50] P. Martinoli, O. Daldini, C. Leemann, and E. Stocker, A.C. quantum interference in superconducting films with periodically modulated thickness, Solid State Commun. **17**, 205 (1975).

[51] P. Martinoli, Static and dynamic interaction of superconducting vortices with a periodic pinning potential, Phys. Rev. B **17**, 1175 (1978).

[52] O.V. Dobrovolskiy, E. Begun, M. Huth, and V.A. Shklovskij, Electrical transport and pinning properties of Nb thin films patterned with focused ion beam-milled washboard nanostructures, New J. Phys. **14**, 113027 (2012).

[53] O.V. Dobrovolskiy and M. Huth, Dual cut-off direct current-tunable microwave low-pass filter on superconducting Nb microstrips with asymmetric nanogrooves, Appl. Phys. Lett. **106**, 142601 (2015).

[54] D. Jaque1, E.M. González, J.I. Martin, J.V. Anguita, and J. L. Vicent, Anisotropic pinning enhancement in Nb films with arrays of submicrometric Ni lines, Appl. Phys. Lett. **81**, 2851 (2002).

[55] O.V. Dobrovolskiy, AC quantum interference effects in nanopatterned Nb microstrips, J. Supercond. Novel Mag. **28**, 469 (2015).

[56] J. Guimpel, L. Civale, F. de la Cruz, J. M. Murduck, and I.K. Schuller, Dimensional phase transition in superconductors with short coherence length, Phys. Rev. B **38**, 2342

(1988).

[57] S.H. Brongersma, E. Verweij, N.J. Koeman, D.G. de Groot, R. Griessen, and B.I. Ivlev, Phys. Rev. Lett. **71**, 2319 (1993).

[58] L.S. Levitov, Phyllotaxis of flux lattices in layered superconductors, Phys. Rev. Lett. **66**, 224 (1991).

[59] L. Balents and D.R. Nelson, Quantum smectic and supersolid order in helium films and vortex arrays, Phys. Rev. B **52**, 12951 (1995).

[60] N. Fogel, M. Mikhailov, Y. Bomze, and O. Yuzephovich, Intrinsic pinning, commensurability, and reentrant behavior on superconducting Mo/Si multilayers, Phys. Rev. B **59**, 3365 (1999).

[61] S. Baily, B. Maiorov, H. Zhou, F. Balakirev, M. Jaime, S. Foltyn, and L. Civale, Smectic vortex phase in optimally doped $YBa_2Cu_3O_7$ thin films, Phys. Rev. Lett. **100**, 027004 (2008).

[62] P.J.W. Moll, L. Balicas, X. Zhu, H.-H. Wen, N.D. Zhigadlo, J. Karpinski, and B. Batlogg, Critical current oscillations in the intrinsic hybrid vortex state of SmFeAs(O,F), Phys. Rev. Lett. **113**, 186402 (2014).

[63] G. Carneiro, Equilibrium vortex-line configurations and critical currents in thin films under a parallel field, Phys. Rev. B **57**, 6077 (1998).

[64] J.J. Barba and J. Albino Aguiar, Bi-dimensional chain-like vortex structure in a mesoscopic superconductor, J. Phys.: Conf. Ser. **150**, 052015 (2009).

[65] G. Karapetrov, M. Milosevic, M. Iavarone, A. Belkin, V. Novosad, and F. Peeters, Transverse instabilities of multiple vortex chains in magnetically coupled $NbSe_2$/permalloy superconductor/ferromagnet bilayers, Phys. Rev. B **80**, 180506 (2009).

[66] G. Piacente, I.V. Schweigert, J.J. Betouras, and F.M. Peeters, Generic properties of a quasi-one-dimensional classical Wigner crystal, Phys. Rev. B **69**, 045324 (2004).

[67] J.E. Galván-Moya and F.M. Peeters, Ginzburg-Landau theory of the zigzag transition in quasi-one-dimensional classical Wigner crystals, Phys. Rev. B **84**, 134106 (2011).

[68] J.E. Galván-Moya, V.R. Misko, and F.M. Peeters, Generic ordering of structural transitions in quasi-one-dimensional Wigner crystals, Phys. Rev. B **90**, 094111 (2014).

[69] W. Ferreira, J. Carvalho, P. Oliveira, G. Farias, and F. Peeters, Structural and dynamical properties of a quasi-one-dimensional classical binary system, Phys. Rev. B **77**, 014112 (2008).

[70] D. Lucena, W.P. Ferreira, F.F. Munarin, G.A. Farias, and F.M. Peeters, Tunable diffusion of magnetic particles in a quasi-one-dimensional channel, Phys. Rev. E **87**, 012307 (2013).

[71] A.V. Straube, R.P.A. Dullens, L. Schimansky-Geier, and A.A. Louis, Zigzag transitions and nonequilibrium pattern formation in colloidal chains, J. Chem. Phys. **139**, 134908 (2013).

[72] J.E. Galván-Moya, D. Lucena, W.P. Ferreira, and F.M. Peeters, Magnetic particles confined in a modulated channel: Structural transitions tunable by tilting a magnetic field, Phys. Rev. E **89**, 032309 (2014).

[73] B. Liu and J. Goree, Phonons in a one-dimensional yukawa chain: Dusty plasma experiment and model, Phys. Rev. E **71**, 046410 (2005).

[74] T.E. Sheridan and A.L. Magyar, Power law behavior of the zigzag transition in Yukawa clusters, Phys. Plasmas **17**, 113703 (2010).

[75] S. Fishman, G. De Chiara, T. Calarco, and G. Morigi, Structural phase transitions in low-dimensional ion crystals, Phys. Rev. B **77**, 064111 (2008).

[76] A. del Campo, G. De Chiara, G. Morigi, M.B. Plenio, and A. Retzker, Structural defects in ion chains by quenching the external potential: the inhomogeneous Kibble-Zurek mechanism, Phys. Rev. Lett. **105**, 075701 (2010).

[77] M. Mielenz, J. Brox, S. Kahra, G. Leschhorn, M. Albert, T. Schaetz, H. Landa, and B. Reznik, Trapping of topological-structural defects in Coulomb crystals, Phys. Rev. Lett. **110**, 133004 (2013).

[78] J.-B. Delfau, C. Coste, and M. Saint Jean, Transverse single-file diffusion near the zigzag transition, Phys. Rev. E **87**, 032163 (2013).

[79] T. Dessup, T. Maimbourg, C. Coste, and M. Saint Jean, Linear instability of a zigzag pattern, Phys. Rev. E **91**, 022908 (2015)

[80] I. Guillamón, R. Córdoba, J. Sesé, J.M. De Teresa, M.R. Ibarra, S. Vieira, and H. Suderow, Enhancement of long-range correlations in a 2D vortex lattice by an incommensurate 1D disorder potential, Nature Phys. **10**, 851 (2014).

[81] S. Bhattacharya and M.J. Higgins, Dynamics of a disordered flux line lattice, Phys. Rev. Lett. **70**, 2617 (1993).

[82] A.E. Koshelev and V.M. Vinokur, Dynamic melting of the vortex lattice, Phys. Rev. Lett. **73**, 3580 (1994).

[83] L. Balents, M.C. Marchetti, and L. Radzihovsky, Nonequilibrium steady states of driven periodic media, Phys. Rev. B **57**, 7705 (1998).

[84] P. Le Doussal and T. Giamarchi, Moving glass theory of driven lattices with disorder, Phys. Rev. B **57**, 11356 (1998).

[85] F. Pardo, F. de la Cruz, P.L. Gammel, E. Bucher, and D.J. Bishop, Observation of smectic and moving-Bragg-glass phases in flowing vortex lattices, Nature (London) **396**, 348 (1998).

[86] C.J. Olson, C. Reichhardt, and F. Nori, Nonequilibrium dynamic phase diagram for vortex lattices, Phys. Rev. Lett. **81**, 3757 (1998).

[87] C. Reichhardt, C.J. Olson, and F. Nori, Dynamic phases of vortices in superconductors with periodic pinning, Phys. Rev. Lett. **78**, 2648 (1997).

[88] C. Reichhardt, C.J. Olson, and F. Nori, Nonequilibrium dynamic phases and plastic flow of driven vortex lattices in superconductors with periodic arrays of pinning sites, Phys. Rev. B **58**, 6534 (1998).

[89] J. Gutierrez, A.V. Silhanek, J. Van de Vondel, W. Gillijns, and V. Moshchalkov, Transition from turbulent to nearly laminar vortex flow in superconductors with periodic pinning, Phys. Rev. B **80**, 140514 (2009).